

PCCP

Accepted Manuscript



This is an *Accepted Manuscript*, which has been through the Royal Society of Chemistry peer review process and has been accepted for publication.

Accepted Manuscripts are published online shortly after acceptance, before technical editing, formatting and proof reading. Using this free service, authors can make their results available to the community, in citable form, before we publish the edited article. We will replace this *Accepted Manuscript* with the edited and formatted *Advance Article* as soon as it is available.

You can find more information about *Accepted Manuscripts* in the [Information for Authors](#).

Please note that technical editing may introduce minor changes to the text and/or graphics, which may alter content. The journal's standard [Terms & Conditions](#) and the [Ethical guidelines](#) still apply. In no event shall the Royal Society of Chemistry be held responsible for any errors or omissions in this *Accepted Manuscript* or any consequences arising from the use of any information it contains.

Tunable Electronic Properties in van der Waals Heterostructure Germanene/Germanane

Run-wu Zhang, Chang-wen Zhang*, Wei-xiao Ji, Feng Li, Miao-juan Ren, Ping Li, Min Yuan, and
Pei-ji Wang

School of Physics and Technology, University of Jinan, Jinan, Shandong, 250022, People's
Republic of China

Abstract:

It is challenging to epitaxially grow germanene on conventional semiconductor substrate. Based on first-principles calculations, we investigate the structural and electronic properties of germanene/germanane heterostructure (HTS). The results indicate that the Dirac cone with nearly linear band dispersion of germanene maintains in the band gap of substrate. Remarkably, the band gap opened in these HTSs can be effectively modulated by the external electric field and strain, along with a very low effective masses and high carrier mobilities. These results provide a route to design high-performance FET operating at room temperature in nanodevices.

Keywords: First-principles calculations; Germanene; Germanane; Band gap; FET

* Corresponding author: C. W. Zhang: zhchwsd@163.com

TEL: ++86-531-82765976; FAX: ++86-531-82765976

1. Introduction

Germanene, a two-dimensional (2D) single-layer Ge crystal, has attracted huge research interest as a versatile platform for investigation of various physical phenomena in high-performance devices [1-2]. Compared with graphene [3-8] and silicene [9-11], it has a more buckled honeycomb structure due to the weakly π - π interaction and distinct coupling of σ and π bonds between Ge atoms, bringing about new physics beyond graphene, [3-8] such as detectable quantum spin Hall (QSH) and valley-polarized quantum anomalous Hall (QAH) state, et al. [12] Meanwhile, due to its linear band dispersion near the Fermi level (E_F) at K point, an extremely high charge carrier mobility is expected, with the value of the order of $10^5 \text{ cm}^2 \text{ V}^{-1} \text{ s}^{-1}$. [13] When it is used as a channel, the transistor can have an ultrafast speed, making it able to operate in the THz frequency range. Together with compatibility with the current semiconductor technology, germanene may be an ideal material for building electronic devices, such as field effect transistor (FET). However, there are still limitations to germanene, for example, the lack of an intrinsic band gap at E_F and low structural stability of germanene, posing a major obstacle for germanene to the use in logic and high-performance switching devices.

Integration of 2D Dirac materials with various metal/semiconductor substrates to form 2D hybrid HTS provides a possible way to create stable germanene nanostructures. Experimentally, Li et al. [14] reported the successful growth of germanene on Pt(111) which has a distorted ($\sqrt{19} \times \sqrt{19}$) superstructure with respect to the substrate. However, further analysis indicates the absence of Dirac cone in germanene due to the strongly orbital hybridization between Ge and substrates. To preserve the intrinsic properties of suspended germanene, the HTSs made by stacking germanene on 2D non-bonding substrates in a chosen sequence – as in building with Lego – with blocks defined with one-atom-plane precision has been proposed to be a possible way. [15-16] For example, Li et al. [15] reported that the germanene on h-BN has an adsorption energy of -130 meV per Ge atom and exhibit the semiconducting behavior. Germanene on MoS_2 has also been proposed, [16] which is p -doped

semiconductor with band gap of 24 meV. Despite these achievements, experimental synthesis of these nanostructures is rather challenging. So, a new substrate is needed for both growing germanene and preserving the Dirac cones in nanoelectronics. [17]

Recently, germanane, a stable full-hydrogenated stoichiometric germanene analogue with a band gap of 1.53 eV, has been successfully synthesized from the topochemical deintercalation of CaGe_2 [18]. Especially, it has a direct band gap of 1.56 eV as well as high carrier mobility. Compared with the substrates BN or MoS_2 , the HTS based on fully-hydrogenated germanene may be more feasible in experiments, due to its compatibility with germanene technology. Here, based on first-principles calculations, we investigate the structural and electronic properties of germanene/germanane HTS. The absence of dangling bonds due to the hydrogen saturation in substrate can render germanene to offer a large band gap (82-120 meV), along with the linear dispersion preserved at Dirac point, and thus low effective mass (EM). Together with compatibility with the current semiconductor technology, germanene is a promising candidate for building FET.

2. Computational methods

All Calculations are performed by using first-principles method as implemented in the Vienna Ab Initio Simulation Package (VASP). [19] We use the generalized gradient approximation (GGA) with the Perdew-Burke-Ernzerhof (PBE) [20] functional to describe the exchange-correlation interaction, which is developed for the calculations of surface systems. To properly take into account the van der Waals (vdW) interactions, the DFT-D2 method [21] is used throughout all the calculations. Also, the projector augmented wave (PAW) method [22] is used to describe the electron-ion interaction, and the dipole corrections are included considering the possible charge redistribution in these HTSs. The convergence criterion of our self-consistent calculations for ionic relaxations is 10^{-5} eV between two consecutive

steps. By using the conjugate gradient method, all atomic positions and the size of the unit cell are optimized until the atomic forces are less than $0.02 \text{ eV } \text{\AA}^{-1}$.

3. Results and Discussion

For the germanene/germanane hybrids, Fig. 1(a) displays 2D germanane with a honeycomb lattice, in which the unit cell comprises two Ge atoms and two H atoms. Different from low buckled germanene, [23] the hydrogenation on Ge atoms forms a strong σ bond between Ge and H atoms, leading to an sp^3 hybridization of Ge atoms, with a large buckled height (h) of 0.73 \AA . Thus, the hydrogenation on Ge atoms breaks down the semimetal character of germanene, resulting in a direct band gap of 1.05 eV , as shown in Fig. 1(b).

The relaxed lattice constant of germanane is 4.06 \AA , indicating a small lattice mismatch ($\sim 0.73\%$) in comparison to germanene.[24] Thus we consider four stacking patterns, such as AA-1, AA-2, AB-1, and AB-2, as shown in Figs. 2(a)-(d). The corresponding relaxed parameters for all HTSs are listed in Table I. It can be seen that the Bernal pattern AB-2 is more stable than other three ones by $\sim 20 \text{ meV}$, accompanied with a smallest interlayer distance of 1.70 \AA . Especially, the interlayer binding energies of all patterns are relatively low, i.e., -37 , -41 , -40 , and -68 meV for AA-1, AA-2, AB-1, and AB-2, respectively, indicating the weak vdW interaction in HTSs. Thus, there is no significant change in the buckling of germanene when deposited on germanane substrate. To further confirm the thermostability of these HTSs, we calculated cohesive (atomization) energies of the heterostructures defined as, $E_c = E_{\text{HTS}} - n_{\text{Ge}}E_{\text{Ge}} - n_{\text{H}}E_{\text{H}}$, where E_{HTS} is the total energy of different conformations, E_{Ge} and E_{H} are the spin-polarized energies of Ge and H atoms, and n_{Ge} and n_{H} are the number of atoms in those structural conformations. We find $E_c = -2.28 \text{ eV}$, suggesting it is feasible in experimental synthesis.

Fig. 3 presents the electronic band structures of all patterns. It can be seen that the symbolic Dirac point of germanene with linear band dispersion are still preserved in these HTSs, indicating that no Ge- $4p_z$ orbitals near E_F involved in the hybridization

with substrate (Figs. 3(a)-(d)). Therefore the characteristics of high carrier mobility in HTSs are expected. Remarkably, we find a large band gap of 82-120 meV opened at Dirac point in all Ge/GeH HTSs, more pronounced than for the room-temperature thermal scale (25 meV). In these cases, the electron EM (m_e^*) and hole EM (m_h^*) at Dirac point can be expressed as [25] $m^* \approx \frac{p}{v_g} \approx \frac{\hbar k}{v_f}$, where k is wave vector and v_f is Fermi velocity. Table II lists the calculated m_e^* and m_h^* along Γ -K and Γ -M directions for all patterns. Obviously, the m_e^* and m_h^* at VBM and CBM for Ge/GeH HTSs are very low, more superior to the previous reported graphene or silicene HTS. [26-27] In these cases, the deduced v_f is considerably high (Table I), comparable to unsuspended germanene (1.7×10^6 m/s). [28] When used as FET, the source and drain electrodes should be connected directly to germanene while the germanene underneath may actually act as a back-gate to precisely control the current on-off ratio. Therefore, germanene may be an appropriate choice/suitable as a substrate for germanene with a larger on-off current ratio in FET.

To gain more insights into the band gap opening in Ge/GeH HTS, we analyze the plane-integrated electron-density difference, $\Delta\rho(z)$ for this interface, as shown in Fig. 4(a). Evident electron-rich and hole-rich regions appear in germanene due to the different electrostatic potential induced by substrate. Further Bader charge analysis indicates that about 0.022 electrons transfer between Ge atoms within germanene layer. This electron redistribution occurring at an interface leads to an intrinsic interface dipole and thus the sublattice symmetry in germanene is broken, resulting in the two sublattices of germanene non-equivalent any longer. According to π -electron tight-binding (TB) model of bipartite lattices, [29] $|E(k)| = \pm\sqrt{\Delta^2 + (\hbar v_F k)^2}$, a nonzero band gap, $E_g = 2\Delta$, is opened. To further understand the electronic charge reorganization, we also estimate the work function (WF) of Ge/GeH HTSs and compare it with that of unsuspended germanene. The WF of germanene substrate is found to be 4.788 eV, while for germanene, it is 4.19 eV, being close to previous reported value.[30] When germanene are integrated into substrate, the WF of HTS is

4.54 eV, which is 0.35 eV higher than that of germanene. Thus, the electron transfer is from germanene to germanane, consistent with the Bader charge analysis. Generally, the definitive quantities for the electrons injection into germanane are determined by the energy level disposition of the ionization potential and the electron affinity potential in HTS, i.e., the valence band maximum (VBM), conduction band minimum (CBM), and WF of germanene. According to the integer charge transfer model, [31,32], the electrical neutrality of germanene is kept when E_F lies in the band gap of germanane, indicating a semiconducting character for all these HTSs.

As revealed above, the band gap opening for these HTSs is induced by the intrinsic interface dipole, an external electric field (E-field) would modulate the electron redistribution at the interface and thus eventually tune the band gap. Fig. 5 displays the band gaps of HTSs as a function of E-field magnitude. For AA-1 and AB-2, we find that the band gap decrease monotonically with the increase of E-field, as shown in Figs. 5(a) and (d). When the E-field is larger enough, the E_F would cross the conduction band, forming self p-doping. While for AA-2 and AB-1, the band gap increases monotonically with the increase of E-field. When E-field ≤ 0.2 V/Å for AA-2 and E-field ≤ 0.4 V/Å for AB-1, although a size band gap preserved at K-point, a self-hole doping could be found. [Figs. 5(b)-(c)]. More importantly, the value of band gap changes nearly linearly with the external E-field, suggesting that the band gaps of HTSs could be efficiently tuned. These features in E-field can be attributed to the E-field inducing a potential difference between the two sublattices of germanene, which is the key factor. [33-34] Explicitly, the E-field induce an electrostatic potential difference between germanene and substrate, and thus the relative energy levels of two layers would separate from each other, causing a shift of energy levels and thus change of band gap.

Another promising route towards the continuously tunable band gap is elastic strain engineering, which is applied to HTSs by changing the lattices as $\varepsilon = (a - a_0)/a_0$, where a (a_0) is the strained (equilibrium) lattice constants of HTSs. Figs. 6(a)-(d) display the band gap change trends with the external strain ε . For AA-1 (Fig. 6(a)), the

band gaps decrease monotonically with the increase of strain $\varepsilon = -3\% \sim -2\%$, while the feature of Dirac cone of germanene preserved still. When the tensile strain is in the range of $-8\% \leq \varepsilon \leq -4\%$, a small gap can be obtained at K-point, while $\varepsilon \leq -8\%$, the band gap of Dirac cone vanished, leading to self-electron doping. However, if the tensile strain reaches $\varepsilon \geq 3\%$, the self-hole doping appears, though a small gap preserved at K-point.

4. Conclusions

In summary, based on first-principles calculations with vdW correction, we study the geometric and electronic properties of Ge/GeH HTSs. It is found that the weak vdW interaction between germanene and substrates remain the Dirac cone of germanene with a linear energy band dispersion in the band gap of germanene. Remarkably, the band gap of all these HTSs can be effectively modulated by the external electric field and strain independent on the stackings of HTSs. These findings indicate that germanene can serve as a high-quality substrate for germanene to realize high-performance FET at room-temperature in nanoelectronics.

Acknowledgments: This work was supported by the National Natural Science Foundation of China (Grant No. 11274143, 11434006, 61172028, and 11304121), and Research Fund for the Doctoral Program of University of Jinan (Grant no. XBS1433).

References

- 1 S. Cahangirov, M. Topsakal, E. Akturk, H. Sahin, and S. Ciraci, *Phys. Rev. Lett.* 2009, **102**, 236804.
- 2 A. O'Hare, F. V. Kusmartsev, and K. I. Kugel, *Nano Lett.* 2012, **12**, 1045.
- 3 K. S. Novoselov, A. K. Geim, S. V. Morozov, D. Jiang, Y. Zhang, S. V. Dubonos, I. V. Gregorieva, and A. A. Firsov, *Science* 2004, **306**, 666.
- 4 A. K. Geim, and K. S. Novoselov, *Nat. Mater.* 2007, **6**, 183.
- 5 A. H. Castro Neto, F. Guinea, N. M. R. Peres, K. S. Novoselov, and A. K. Geim, *Rev. Mod. Phys.* 2009, **81**, 109.
- 6 J. X. Zheng, L. Wang, Ruge Quhe, Q. H. Liu, H. Li, D. P. Yu, W. N. Mei, J. J. Shi, Z. X. Gao, J. Lu, *Sci. Rep.* 3,1314; DOI:10.1038/srep01314 (2013).
- 7 Y. Y. Wang, Z. Y. Ni, Q. H. Liu, Ruge Quhe, J. X. Zheng, M. Ye, D. P. Yu, J. J. Shi, J. B. Yang, J. Li, *Advanced Functional Materials*, 2015, **25**(1), 68.
- 8 M. Ye, Ruge Quhe, J. X. Zheng, Z. Y. Ni, Y. Y. Wang, Y. K. Yuan, Geoffrey Tse, J. Shi, Z. X. Gao, J. Lu, *Physica E* ,2014, **59**, 60.
- 9 R. W. Zhang, C. W. Zhang, W. X. Ji, S. J. Hu, S. S. Yan, S. S. Li, P. Li, and Y. S. Liu, *J. Phys. Chem. C* 2014, **118**, 25278.
- 10 B. Lalmi, H. Oughaddou, H. Enriquez, A. Kara, S. Vizzini, B. Ealet, and B. Aufray, *Appl. Phys. Lett.* 2010, **97**, 223109.
- 11 P. Vogt, P. D. Padova, C. Quaresima, J. Avila, E. Frantzeskakis, M. C. Asensio, A. Resta, B. Ealet, and G. L. Lay, *Phys. Rev. Lett.* 2012, **108**, 155501.
- 12 C. C. Liu, W. Feng, and Y. Yao, *Phys. Rev. Lett.* 2011, **107**, 076802.
- 13 Z. G. Shao, X. S. Ye, L. Yang, and C. L. Wang, *J. Appl. Phys.* 2013, **114**, 093712.
- 14 L. F. Li, S. Z. Lu, and J. B. Pan, *Advanced Materials* 2014, **26**, 4820.
- 15 L. Y. Li, and M. W. Zhao, *Phys. Chem. Chem. Phys.* 2013, **15**, 16853.
- 17 Y. Ma, Y. Dai, and B. Huang, *J. Phys. Chem. L* 2013, **4**, 2471.
- 18 E. Bianco, S. Butler, S. Jiang, O. D. Restrepo, W. Windl, and J. E. Goldberger, *ACS Nano* 2013, **7**, 4414.
- 19 G. Kresse, and J. Furthmuller, *Phys. Rev. B* 1996, **54**, 11169.

- 20 J. P. Perdew, and Y. Wang, *Phys. Rev. B* 1992, **45**, 13244.
- 21 S. Grimme, *J. Comput. Chem.* 2006, **27**, 1787.
- 22 G. Kresse, and D. Joubert, *Phys. Rev. B* 1999, **59**, 1758.
- 23 H. Haugen, D. Huertas-Hernando, and A. Brataas, *Phys. Rev. B* 2008, **77**, 115406.
- 24 S. S. Li, C. W. Zhang, W. X. Ji, F. Li, P. J. Wang, S. J. Hu, S. S. Yan, Y. S. Liu, *Phys. Chem. Chem. Phys.* 2014, **16**, 15968.
- 25 K. S. Novoselov, A. K. Geim, S. V. Morozov, D. Jiang, M. I. Katsnelson, I. V. Grigorieva, S. V. Dubonos, and A. A. Firsov, *Nature* 2005, **438**, 197.
- 26 K. Chen, X. Wan, and Xu, *J. Mater. Chem. C* 2013, **1**, 4869.
- 27 M. Houssa, B. van den Broek, E. Scalise, G. Pourtois, V. V. Afanas'ev, and A. Stesmans, *Phys. Chem. Chem. Phys.* 2013, **15**, 3702.
- 28 T. P. Kaloni, and U. J. Schwingenschlögl, *J. Appl. Phys.* 2013, **114**, 184307.
- 29 Y. Fan, M. Zhao, Z. Wang, X. Zhang, and H. Zhang, *Appl. Phys. Lett.* 2011, **98**, 083103.
- 30 H. Sahin, and F. M. Peeters, *Phys. Rev. B: Condens. Matter Mater. Phys.* 2013, **87**, 085423.
- 31 L. Chen, L. Wang, Z. Shuai, and D. J. Beljonne, *J. Phys. Chem. Lett.* 2013, **4**, 2158.
- 32 T. Hu, and I. C. Gerber, *J. Phys. Chem. C* 2013, **117**, 2411.
- 33 Z. Y. Ni, Q. H. Liu, K. C. Tang, J. X. Zheng, J. Zhou, R. Qin, Z. X. Gao, D. P. Yu, and J. Lu, *Nano Lett.* 2012, **12**, 113.
- 34 N. D. Drummond, V. Zólyomi, V. I. Fal'ko, *Phys. Rev. B* 2012, **85**, 075423.

Table I Detailed structural and electronic information for Ge/GeH HTSs, including interlayer binding energy per Ge atom (meV), the interlayer spacing d , band gap (meV), as well as the EM of electron (m_e) and hole (m_h) at K point along $K-M$ and $K-\Gamma$ directions. Here, m_0 is the free electron mass.

Fig.1 Relaxed geometric structure for germanane (a), and band structure (b) of germanane. The red dot lines plotted in (b) are calculated with TB simulation.

Fig. 2 The optimized structures of the HTSs, (a) AA-1, (b) AA-2, (c) AB-1, (d) AB-2. The greyish green ball represent Ge atoms, white ball represent hydrogen atoms, respectively.

Fig. 3 Band structures of the Ge/GeH HTSs for patterns (a) AA-1, (b) AA-2, (c) AB-1, (d) AB-2, respectively.

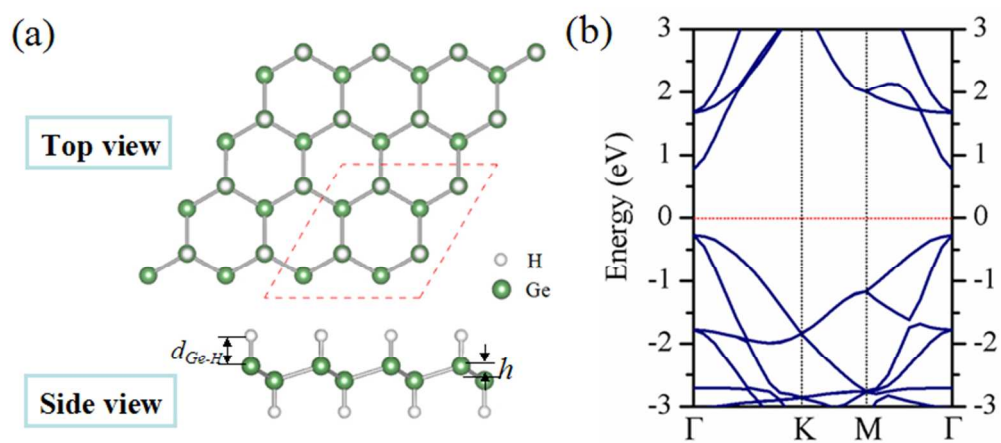
Fig. 4 (a) is plane-integrated electron density difference, $\Delta\rho(r)$, for Ge/GeH HTSs. (b) is the schematic energy level disposition for the pristine germanene and germanane monolayer. Here, the plane-averaged charge density difference $\Delta\rho(z)$ induced by substrate can be expressed as $\Delta\rho(z) = \rho_{\text{total}} - \rho_{\text{germanene}} - \rho_{\text{germanane}}$, where ρ_{total} , $\rho_{\text{germanene}}$, and $\rho_{\text{Germanane}}$ are the total charge densities of Ge/GeH, germanene, and germanane, respectively.

Fig. 5 The trend of band gaps of HTSs as a function of external E-Field for (a) AA-1, (b) AA-2, (c) AB-1, (d) AB-2, respectively.

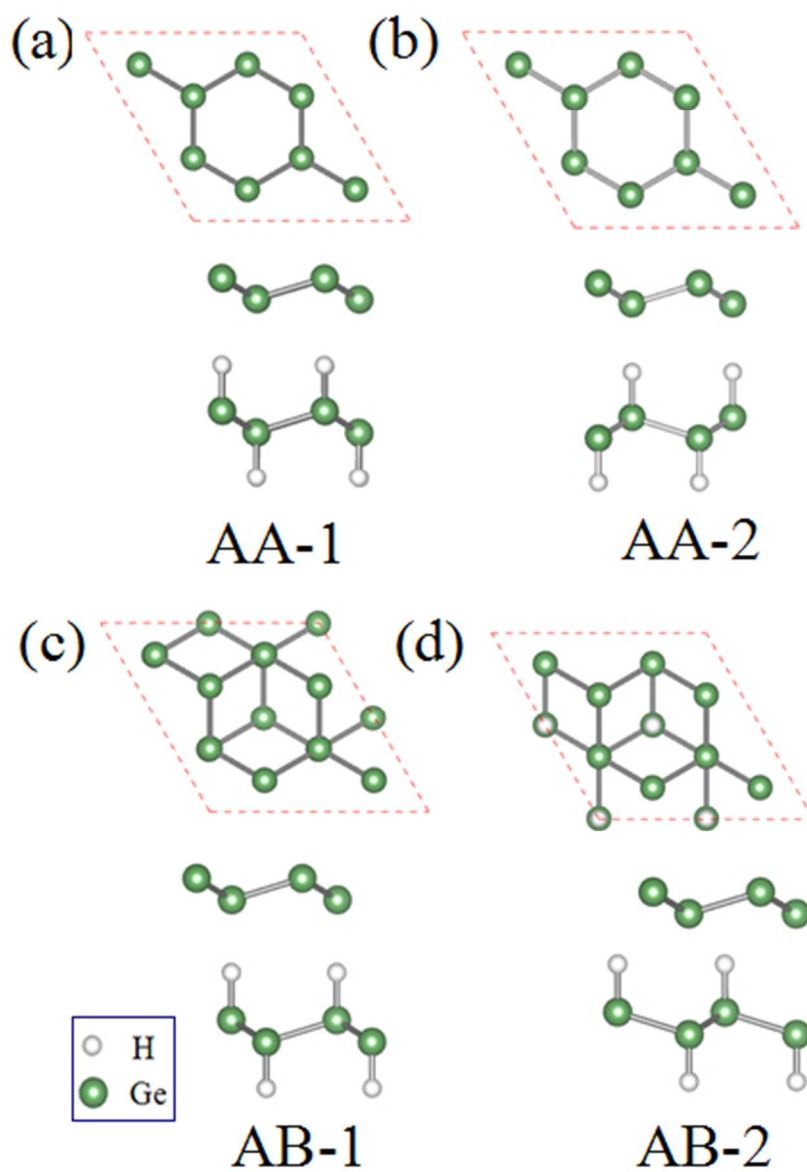
Fig. 6 The trend of band gaps of HTSs as a function of strain for (a) AA-1, (b) AA-2, (c) AB-1, (d) AB-2, respectively.

Table I Detailed structural and electronic information for Ge/GeH HTSs, including interlayer binding energy per Ge atom (meV), the interlayer spacing d , band gap (meV), as well as the EM of electron (m_e) and hole (m_h) at K point along K–M and K– Γ directions. Here, m_0 is the free electron mass.

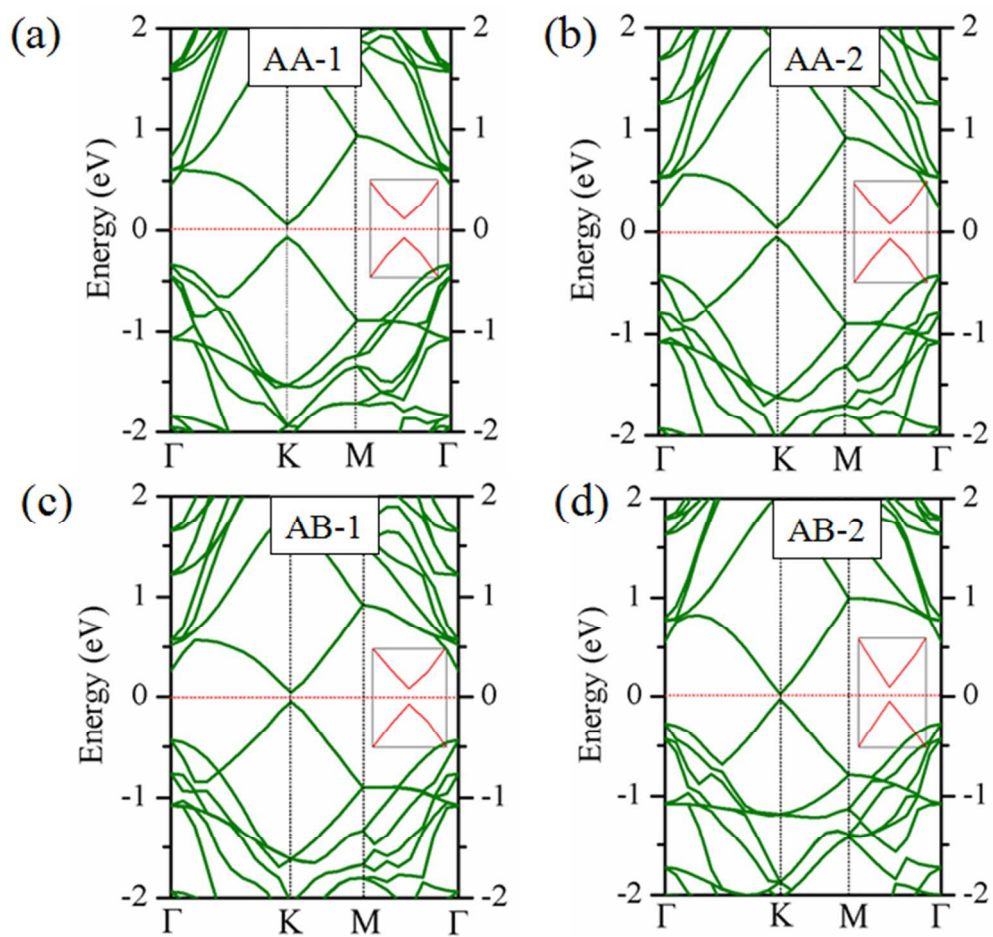
Pattern	E_b	$d(\text{\AA})$	E_g	$m_e^{\text{K}\Gamma}$	m_e^{KM}	$m_h^{\text{K}\Gamma}$	m_h^{KM}	$V_f(\text{max})$
<i>AA-1</i>	-37	2.31	120	$0.0924m_0$	$0.1040m_0$	$0.0953m_0$	$0.1053m_0$	0.3377×10^6
<i>AA-2</i>	-41	2.41	89	$0.0839m_0$	$0.0934m_0$	$0.0866m_0$	$0.0949m_0$	0.3544×10^6
<i>AB-1</i>	-40	2.42	87	$0.0859m_0$	$0.0924m_0$	$0.0891m_0$	$0.0941m_0$	0.3503×10^6
<i>AB-2</i>	-68	1.70	52	$0.0691m_0$	$0.0796m_0$	$0.0668m_0$	$0.0767m_0$	0.3972×10^6



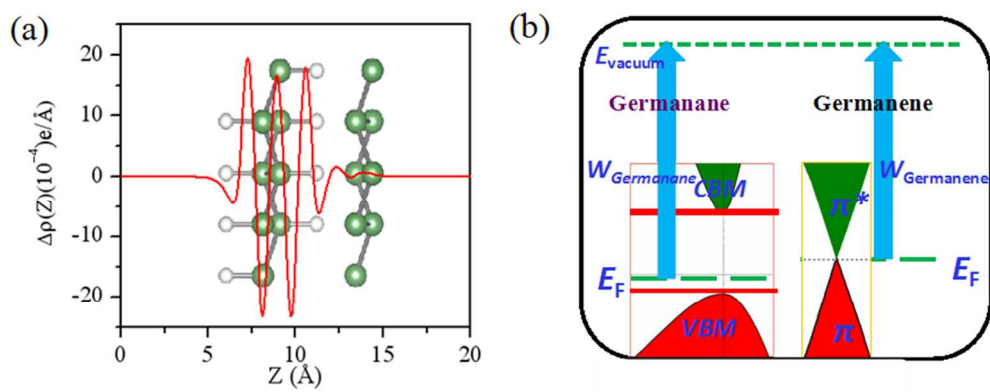
207x93mm (96 x 96 DPI)



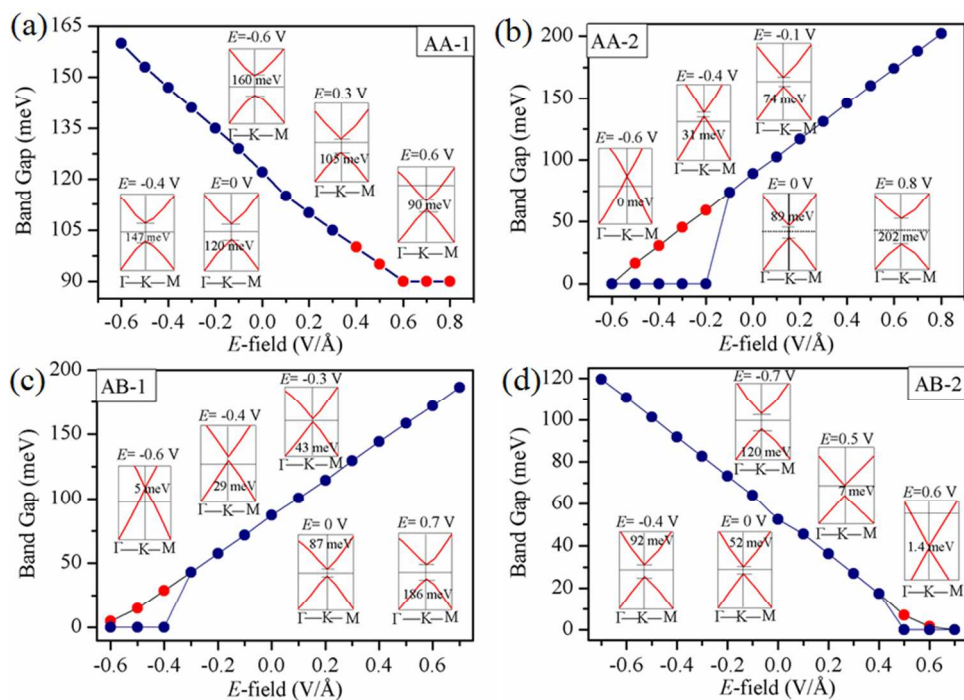
115x165mm (96 x 96 DPI)



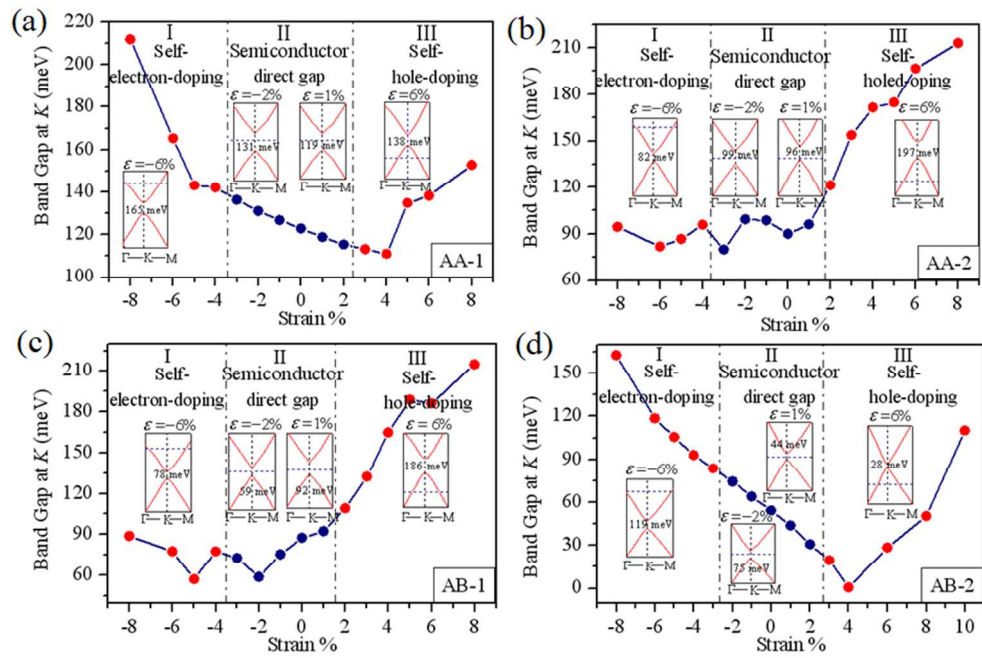
179x169mm (96 x 96 DPI)



234x95mm (96 x 96 DPI)



250x177mm (96 x 96 DPI)



252x168mm (96 x 96 DPI)